APL Materials

RESEARCH ARTICLE | APRIL 18 2024

Ultrafast THz emission spectroscopy of spin currents in the metamagnet FeRh

Yinchuan Lv; Soho Shim ; Jonathan Gibbons ; Axel Hoffmann ; Nadya Mason ; Fahad Mahmood

APL Mater. 12, 041121 (2024)
https://doi.org/10.1063/5.0201789

APL Materials ARTICLE pubs.aip.org/aip/apm

Ultrafast THz emission spectroscopy of spin currents in the metamagnet FeRh

Cite as: APL Mater. 12, 041121 (2024); doi: 10.1063/5.0201789
Submitted: 31 January 2024 • Accepted: 2 April 2024 •
Published Online: 18 April 2024

Yinchuan Lv,[1,2] Soho Shim,[1,2] Jonathan Gibbons,[3,4,5,a)] Axel Hoffmann,[1,2,3,4] Nadya Mason,[1,2] and Fahad Mahmood[1,2,b)]

AFFILIATIONS

[1] Department of Physics, University of Illinois at Urbana-Champaign, Urbana, 61801 Illinois, USA
[2] Materials Research Laboratory, University of Illinois at Urbana-Champaign, Urbana, 61801 Illinois, USA
[3] Department of Materials Science and Engineering, University of Illinois at Urbana-Champaign, Urbana, Illinois 61801, USA
[4] Materials Science Division, Argonne National Laboratory, Lemont, Illinois 60439, USA
[5] Physics Department, University of California, San Diego, California 92093, USA

Note: This paper is part of the Special Topic on Ultrafast Materials Science: Coherence and Dynamics.
[a)] **Present address:** Western Digital Research Center, Western Digital Coproration, San Jose, California 95119, USA.
[b)] **Author to whom correspondence should be addressed:** fahad@illinois.edu

ABSTRACT

Heterostructures of ferromagnetic (FM) and noble metal (NM) thin films have recently attracted considerable interest as viable platforms for the ultrafast generation, control, and transduction of light-induced spin currents. In such systems, an ultrafast laser can generate a transient spin current in the FM layer, which is then converted to a charge current at the FM/NM interface due to strong spin–orbit coupling in the NM layer. Whether such conversion can happen in a single material and how the resulting spin current can be quantified are open questions under active study. Here, we report ultrafast THz emission from spin–charge conversion in a bare FeRh thin film without any NM layer. Our results highlight that the magnetic material by itself can enable spin–charge conversion in the same order as that in a FM/NM heterostructure. We further propose a simple model to estimate the light-induced spin current in FeRh across its metamagnetic phase transition temperature. Our findings have implications for the study of the ultrafast dynamics of magnetic order in quantum materials using THz emission spectroscopy.

There has been considerable interest recently in establishing viable platforms for the ultrafast generation and detection of spin current through spin–charge interconversion. Notable examples of such platforms are heterostructures of ferromagnetic (FM) and noble metal (NM) materials in which the dynamics of spin current can, in principle, be probed using coherent time-domain THz emission spectroscopy.[1–6] When pumped by an ultrafast laser pulse, the FM layer, with its magnetization pointing in-plane, launches a spin current transverse to its magnetization direction. As the spin current propagates across the FM/NM interface, strong spin–orbit coupling in the NM layer converts it into a transient charge current via the inverse spin Hall effect (ISHE)[1–5] or the Rashba–Edelstein effect.[6]

In the case of ISHE, $\vec{j_c}(z) = \gamma(2e/\hbar)[\vec{j_s}(z) \times \vec{\sigma}]$,[7] where j_s and j_c denote the induced spin current and charge current, γ is the spin Hall angle, and $\vec{\sigma}$ is the spin direction. The lifetime of this transient charge current is on the order of a few ps, which results in a radiation spectrum with frequencies in the 0.1 to 10 THz range. This method of generating THz relies on the strong spin–orbit coupling strength of the adjacent NM capping layer. Although ISHE has been observed in -ferromagnets such as permalloy (Py) and yttrium iron garnet (YIG) through the spin Seebeck effect or spin pumping,[7,8] the study of THz generation from a single FM metal thin layer (without any adjacent NM layer) by ISHE remains quite limited[9] and often results in very small THz emission.[6] FM metals with large intrinsic spin–orbit coupling (SOC) can have a transverse charge current

converted from a laser-induced spin current. This approach to measure spin currents through THz generation can also be extended to antiferromagnetic (AFM) metals with large spin–orbit coupling, in which large spin Hall effects (comparable to those of Pt) have been shown.[10–12]

FeRh is a metal which undergoes a first-order metamagnetic phase transition from antiferromagnet (AFM) to ferromagnetic ordering (FM) above room temperature, with an accompanying lattice expansion of about 1%.[13,14] Depending on the thickness of the FeRh film, chemical composition, and local strain, the transition temperature can vary by tens of Kelvin.[15–18] This metamagnetic transition makes FeRh a promising candidate for understanding coupled lattice and spin dynamics at ultrashort time scales. Seminal pump–probe and magneto-optical Kerr (MOKE) experiments have shown that laser pulses can induce FM domains in the AFM phase of FeRh within sub-picoseconds.[19,20] Later, several experimental and theoretical studies investigated the mechanism behind this transition from AFM to FM order.[21–24] Recent work using time-resolved photo-electron momentum microscopy suggests that a change in the electronic structure causes this first-order transition,[25] while another study using MOKE in high magnetic fields suggests that the magnetization formation and a structural change take place simultaneously.[26]

Regardless of the mechanism of the transition from the AFM to the FM phase, the large SOC in FeRh allows for an investigation of light-induced spin currents and THz generation via ISHE in both the AFM and FM phases in a single material. THz emission from FeRh based heterostructures was recently reported by Seifert *et al.* at temperatures above the phase transition.[2] This THz emission decreases at a lower temperature but shows a lack of temperature hysteresis that is distinct from a SQUID magnetic moment measurement.[27] Li *et al.* further inspected the observed absence of temperature hysteresis and attributed it to the expansion of FM domains inside FeRh after photo-excitation.[28] In another recent study,[33] THz emission was observed in FeRh capped with gold using a double pump scheme. The study suggests that there is an intrinsic latency between laser-induced heating and emergent ferromagnetic order. Similarly, Awari *et al.*[9] demonstrated that optical pump-THz emission can be a good probe for ultrafast magnetization dynamics in bare FeRh. Despite these studies, the origin of the THz emission in bare FeRh and whether the AFM phase of FeRh can host light-induced spin currents are not fully clear.

In this paper, we use ultrafast THz emission spectroscopy across a broad temperature range to study the dynamics of THz emission from a bare FeRh thin film in both the FM and AFM phases. We excite an epitaxial FeRh film grown on a MgO substrate with an ultrafast infrared pump, which transiently demagnetizes the sample and generates THz pulses. By examining the sample orientation and pump polarization dependence of the emitted THz, we attribute the ISHE to be the dominant contributor to THz emission in the FM and AFM phases of bare FeRh. THz emission spectroscopy in this fashion serves as a contact-less probe of the spin current in FeRh.

Epitaxial FeRh samples are grown using magnetron co-sputtering of FeRh from elemental targets on an (100) MgO substrate. First, the MgO substrate is pre-annealed *in situ* for 1 h at a temperature of 850 °C to ensure that the substrate is clean and dry. Then, the 15 nm FeRh film is co-sputtered at 450 °C. We sputter with a nominal composition of ~47.5% Fe and 52.5% Rh, optimized to produce a robust metamagnetic transition in the FeRh. Finally, the film is annealed for 1 h at 650 °C to relax the film strain and allow the FeRh to develop a nicely ordered crystal structure. The sample is allowed to cool overnight *in situ* before use.

Figure 1(a) shows a schematic of the THz emission spectroscopy setup. When illuminated by a 1030 nm ultrashort optical pulse, the MgO/FeRh sample emits bursts of THz radiation, which we measure in the far-field using standard time-domain electro-optic sampling (EOS). The sample is kept in a closed-cycle helium optical cryostat under zero external magnetic field and is excited by linearly polarized laser pulses (a duration of 160 fs, a center wavelength of 1030 nm, and a fluence of 0.1–0.5 mJ/cm^2). The IR pump is obtained from an Yb:KGW amplifier (PHAROS—Light Conversion) and is normally incident from either side of the sample (the beam diameter at the sample is 2 mm FWHM). The emitted THz field is collected by an off-axis parabolic mirror and focused onto a 0.5 mm thick CdTe(110) crystal. The THz electric field as a function of time is determined by EOS using a balanced detection scheme. Note that CdTe(110) has the same structure as the electro-optic crystal GaP but with a larger linear electro-optic coefficient.[29] As such, CdTe(110) has been used to measure the THz electric field using EOS in a variety of studies with a laser wavelength of 1030 nm.[30,31]

Figure 1(b) shows the emitted THz field from a 15 nm FeRh thin film as a function of EOS time at room temperature in the absence of a magnetic field. The FeRh is in the FM phase (the metamagnetic transition point is estimated to be 285 K for our sample) and magnetized before the experiment. Blue and pink traces represent the THz emission when the sample is excited from the FeRh side (blue trace) and from the MgO substrate side (pink trace). When the pump is incident from the MgO side, a single-cycle THz pulse is produced with a negative maximum. When the sample is inverted about the magnetization axis, the generated waveform has the same shape but a reversed sign and a slightly larger magnitude, following the same behavior as observed in other NM/FM bilayer systems.[1,2] This observation implies that the dominant THz emission mechanism in bare FeRh is of an electric dipole nature instead of a magnetic dipole nature, as the latter should remain unchanged when flipping the sample and should be much smaller in magnitude than the electric counterpart.[28,32] However, we do notice a small difference in the amplitude of the THz emission before and after flipping the sample. This can be an indication of the co-existence of electric and magnetic dipole radiation, with electric dipole radiation being the dominant mechanism. Figure 1(c) shows the sample orientation dependence of the measured THz signal. As illustrated in the figure, we define 0° as when the FeRh magnetization is aligned parallel to the $(1\bar{1}0)$ axis of the CdTe crystal. By making an in-plane rotation of the FeRh sample, we observe that the EO signal flips sign when the sample is rotated by 180° and reaches its maximum again after a full-cycle of rotation. The cosine dependence of the EO signal implies that the polarization of the emitted THz field is always perpendicular to the magnetization direction. We keep the sample orientation at 0° and pump from the FeRh side to achieve an optimal signal level for the rest of this study. Pump polarization-dependent THz emission in Fig. 1(d) shows that in the FM phase (300 K), near the metamagnetic transition point (240 K), and in

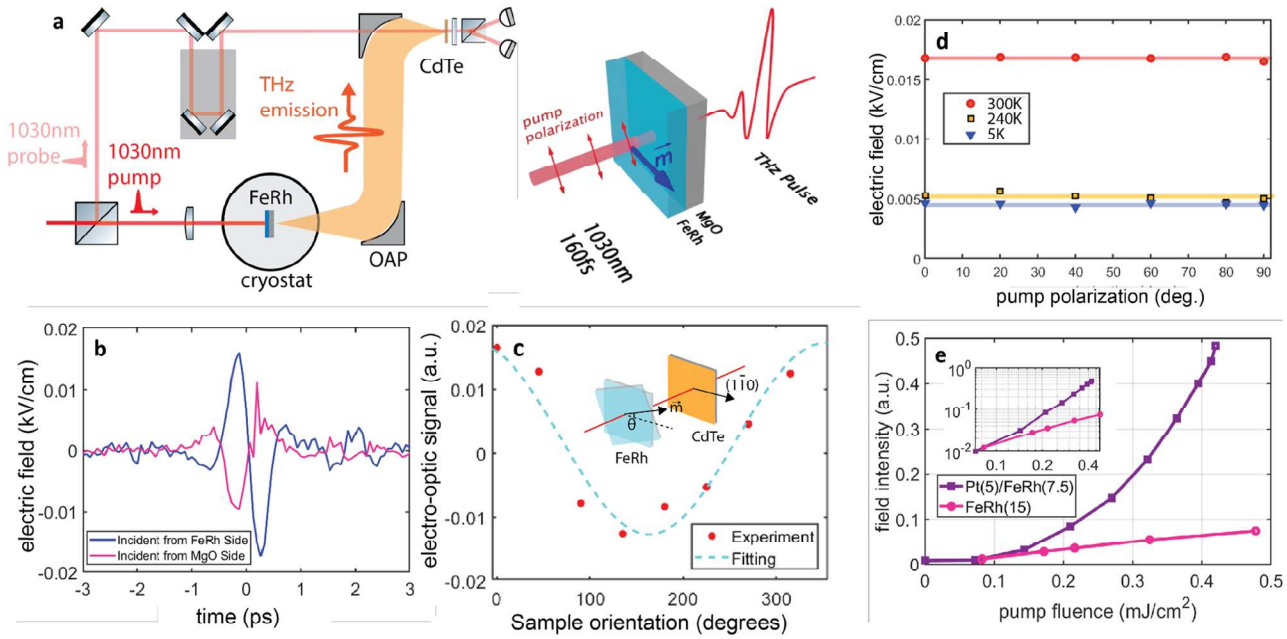

FIG. 1. (a) Left: Schematic of the THz emission spectroscopy setup. Right: THz emission configuration. A 1030 nm, 160 fs long pump pulse is normally incident on an FeRh thin film on an MgO substrate. The emitted THz is detected using electro-optic sampling in a CdTe crystal with a balanced detection scheme. The blue arrow $\vec{m}$ denotes the magnetization direction, while the red arrows represent the incident pump polarization. A transient THz pulse is emitted with polarization normal to $\vec{m}$. (b) The time-domain electric field profile of the emitted THz pulse with the IR laser pump incident from the FeRh side (blue) and the MgO side (pink). For the rest of the results in the paper, the 1030 nm pump is incident on the sample from the FeRh side. (c) Sample orientation dependent THz emission from the 15 nm thick FeRh film at room temperature. Here, we define 0° as the FeRh magnetization aligned parallel to the $(1\bar{1}0)$ axis of the CdTe detection crystal. (d) Pump polarization dependence of the emitted THz field at three different temperatures: 5 K (blue), 240 K (yellow), and 300 K (red). 0° indicates the pump polarization parallel to the FeRh magnetization $\vec{m}$, and 90° corresponds to the pump polarization normal to $\vec{m}$. (e) Pump fluence dependence of the emitted THz field at 295 K. THz emissions from Pt/FeRh (purple) and bare FeRh (pink) show different power-law dependencies on pump fluence. Inset: same plot on a log–log scale.

the AFM phase (5 K), the FeRh THz emission strength is independent of the pump polarization. Both the sample orientation and pump polarization results show key features of the ISHE mechanism: the polarization of the emitted THz field from bare FeRh is always normal to the magnetization direction and independent of the pump polarization, as illustrated in Fig. 1(d). The pump fluence dependent study is also performed, as shown in Fig. 1(e). At room temperature, the strength of the THz field from the FeRh thin film scales linearly with pump fluence, in contrast to the quadratic dependence observed in Pt capped FM-order FeRh as reported in the previous study.[2] No saturation is observed up to the highest pump fluence of 0.5 mJ/cm^{2}in our experiment.

To investigate spin dynamics in FeRh for both AFM and FM magnetic ordering, we first examined THz emission across a range of sample temperatures under zero external magnetic fields [Fig. 2(a)]. At room temperature, the emitted THz field strength is on the order of a few V/cm for a pump fluence of ~0.4 mJ/cm^2. The strength of the THz field is found to decrease linearly as the temperature decreases [Fig. 2(c)]. Such an effect is in agreement with previous studies[21,33,34] in which AFM domains inside FeRh start to nucleate and expand during the first-order phase transition, leading to a drop in the net magnetization of the film. Below 285 K, we observed a sharp decrease in the emitted THz field strength, consistent with the onset of AFM order in bulk FeRh.

The corresponding charge current that leads to the THz emission can be derived by using the electric dipole approximation and integrating the measured THz field over time. The charge current follows the same temperature dependence as the THz field, which starts to quench around room temperature and suddenly reaches a small non-zero value for all temperatures below 285 K, i.e., in the AFM phase [Fig. 2(b)]. In the AFM phase, the emitted THz field is much smaller than that in the FM state. As shown in the inset of Figs. 2(a) and 2(b), the THz waveform and the associated transient current in the AFM state coincide with those in the FM state for the first picosecond of the emission. However, for later times, the transient current in the AFM state is out of phase with that in the FM state. This can be an indication of more than one THz emission mechanism in FeRh.[35,36] To make this trend clearer, we plot the integrated THz field strength as a function of temperature in Fig. 2(c). A clear hysteresis can be seen between the zero-field cooling (blue curve) and zero-field heating (red curve), with a temperature difference of about 20 K. Considering the low fluence of our pump pulse (~0.4 mJ/cm ^{2}), the photoexcitation is not strong enough to induce significant nucleation of FM domains inside the FeRh bulk. Hence, the observation of temperature hysteresis is in agreement with previous studies.[9]

In contrast to previous studies of THz emission in FeRh/Pt bilayers,[2,28] none of the bare FeRh samples we studied here show a

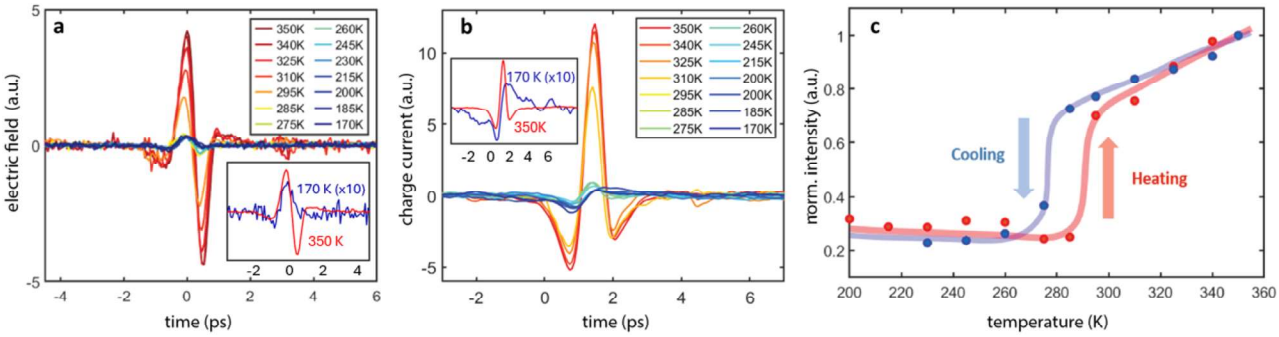

FIG. 2. (a) Temperature dependence of the emitted THz field from a 15 nm bare FeRh film. Inset: comparison between the THz electric field at 320 K (red) and at 170 K (blue). The field at 170 K is scaled 10 times for clarity. (b) Temperature dependence of the transient charge current j_c derived from the emitted THz field profiles shown in (a) by taking the integral of the electric field with respect to time. Inset: Comparison between the transient charge current at 320 K (red) and 170 K (blue). The current at 170 K is scaled 10 times for clarity. (c) Emitted THz field under zero field heating (red) and cooling (blue). Each data point represents the integrated field intensity normalized to the highest measured value.

complete quenching of THz emission at low temperatures. One possible mechanism for the non-vanishing THz emission at low temperatures is collinear magnetic difference frequency generation (DFG), a phenomenon observed in bare AFM insulators possessing zero magnetization, such as (111) oriented NiO.[37,38] A distinguishing feature of THz emission by magnetic DFG is a strong dependence on the pump polarization, attributed to the unequal nonlinear susceptibility tensor components at different pump polarizations. Yet, as shown in Fig. 1(c), the emitted THz field in bare FeRh is independent of pump polarization at all temperatures, which rules out magnetic DFG as the source of THz emission. Possible THz emission mechanisms obeying the same symmetry properties as we observe are the anomalous Nernst effect (ANE), anomalous Hall effect (AHE), and ISHE. The ANE accounts for a transient spin-polarized charge current induced by a sub-picosecond electron temperature gradient, which is commonly seen in a FM thin film.[35,39] The AHE accounts for the conversion of laser-induced longitudinal charge current to a transient transverse current, which generates THz emission and is observed at a FM/dielectric interface.[40] Previous THz emission studies have shown that it is challenging to disentangle the contribution from ANE, AHE, and ISHE, as all three mechanisms have the same symmetry properties for THz emission.[35] However, according to theory calculations,[36] both the AHE and ANE are expected to be suppressed once the FeRh is cooled down below the transition temperature, while the spin-Hall conductivity should remain non-zero and flip sign. Therefore, we rule out AHE and ANE as the THz emission mechanisms for the AFM phase of FeRh. As shown in the inset of Figs. 2(a) and 2(b), both the THz waveform and transient charge current change shape across the transition temperature. The THz field flips the sign after 0 ps, while the transient charge current flips the sign after 1 ps as the FeRh goes across the transition temperature. This observation can be explained by a shift in the weight of contributions from the three mechanisms. In the FM phase, ANE, AHE, and ISHE all contribute to the THz emission, while in the AFM phase, only ISHE contributes to the THz emission. At last, we exclude the possibility of a thermally induced AFM-FM phase transition at temperatures far below the transition temperature. The critical fluence required to drive the phase transition at a temperature 15 K below the transition temperature is ten times larger than the fluence used in our experiment[9,19,41] and should be larger at even lower temperatures.

We note that epitaxial FeRh grown on a MgO substrate has been known to exhibit a narrow FM layer at the substrate interface that persists well into the AFM phase.[16,18,42,43] Several groups have reported that a combination of strain and Fe deficiency leads to the formation of a few nm thick FM layers at the MgO–FeRh interface, even 80 K below the transition temperature.[16,18,42–45] Based on this, one possibility for the temperature-independent THz emission below the transition temperature is the demagnetization of residual FM FeRh domains near the MgO substrate and the following spin-to-charge current conversion inside FeRh through ISHE. In this case, the ultra-fast IR pump demagnetizes the FM layer, creating a thermal gradient along the propagation direction. The combined effect of laser demagnetization and the spin Seebeck effect launches a spin current into the FeRh bulk within hundreds of fs, which is converted into a transient charge current via ISHE.[5,46,47] This interpretation is consistent with previous SQUID measurements[48] and the symmetry properties of our THz emission data.

We note that determining the relative contributions of the ANE, AHE, and ISHE in the THz emission from the FM FeRh sample requires a careful analysis of the induced temperature gradient and measurements on samples with different thicknesses. Such studies are beyond the scope of the present work, where, for simplicity, we focus on the ISHE as the dominant THz emission mechanism at all temperatures. We further assume that the temperature dependence of the generated spin current only comes from a change in the net magnetization, i.e., from a change in the size of the ferromagnetic domain. Based on this simplified model, we propose a scheme to extract the light-induced spin current in FeRh from the measurement. The measured THz field in the frequency domain is related to the spin current by[1]

$$\vec{E}(\omega) = eZ(\omega)\gamma\lambda_{rel}j_S(\vec{\omega}). \quad (1)$$

Here, $\vec{E}(\omega)$ is the emitted THz field, $Z(\omega)$ is the impedance of the thin film, γ and λ_{rel} are the material-dependent spin Hall angle and

spin-relaxation length, respectively, and $j_s(\omega)$ is the light-induced spin current. With the knowledge of $Z(\omega)$, γ, and λ_{rel}, one can extract $j_s(\omega)$ as a function of temperature.

To measure $Z(\omega)$, we performed time-domain THz spectroscopy on the FeRh thin film in reference to a bare MgO substrate. The measured complex conductivity $\sigma(\omega)$ is shown in Figs. 3(a) and 3(b). We also take into account that the absorption at frequencies much greater than the setup's spectral range, which contributes to the measured imaginary part of the complex conductivity, i.e., $\sigma_2(\omega)$. Such excitation will contribute to the low frequency dielectric constant that should be removed from $\sigma_2(\omega)$. Due to the Kramers–Kronig relation for optical conductivity as stated below, a finite $\sigma_1(\omega)$ at high frequencies (absorption) can lead to a measurable $\sigma_2(\omega)$ at low frequencies,

$$\sigma_2(\omega) = -\frac{2\omega}{\pi}\mathcal{P}\int_0^\infty \frac{\sigma_1(\omega')}{\omega'^2-\omega^2}\,\mathrm{d}\omega'. \tag{2}$$

For FeRh, the complex conductivity $\sigma(\omega)$ at low frequencies is Drude-like and can be written as

$$\sigma(\omega) = \frac{S\tau}{1-i\omega\tau} - i(\epsilon_\infty - 1)\epsilon_0\omega, \tag{3}$$

where S is the Drude spectral weight, τ is the scattering mean free time, and $i(\epsilon_\infty - 1)\epsilon_0\omega$ accounts for the high-frequency excitation contribution to the low-frequency spectrum. In Figs. 3(a) and 3(b), we plot the real part of conductivity, $\sigma_1(\omega)$, and the imaginary part of conductivity, $\sigma_2(\omega)$, for the 15 nm FeRh measured between 170 and 325 K. $\sigma_1(\omega)$ for each temperature can be fit to $\sigma_1(\omega) = S\tau/(1+\omega^2\tau^2)$ to estimate the parameters S and τ from which $\sigma_2(\omega)$ is calculated. The high-frequency absorption $i(\epsilon_\infty - 1)\epsilon_0\omega$ is subtracted from $\sigma_2(\omega)$ during our calculation. The temperature dependent DC conductivity of FeRh can be obtained by extrapolating $\sigma_1(\omega)$ at the limit of $\omega = 0$ and is shown in Fig. 3(c). The impedance of the FeRh film can be extracted by integrating $\sigma_{DC}(T)$ over the thickness of the FeRh thin film and fitting it to a model developed in previous theoretical work.[49] The temperature dependent $Z(\omega)$ is shown in Fig. 3(d). A change in the impedance around 325 K is observed across the AFM–FM transition point. This sudden change can be attributed to an increased density of states of the delocalized *sp* electrons near the chemical potential and a smaller spin fluctuation in the FM state.[22,50] As a result, both the electron density and the electron mean free path increase across the transition temperature, leading to a reduced impedance at 325 K.

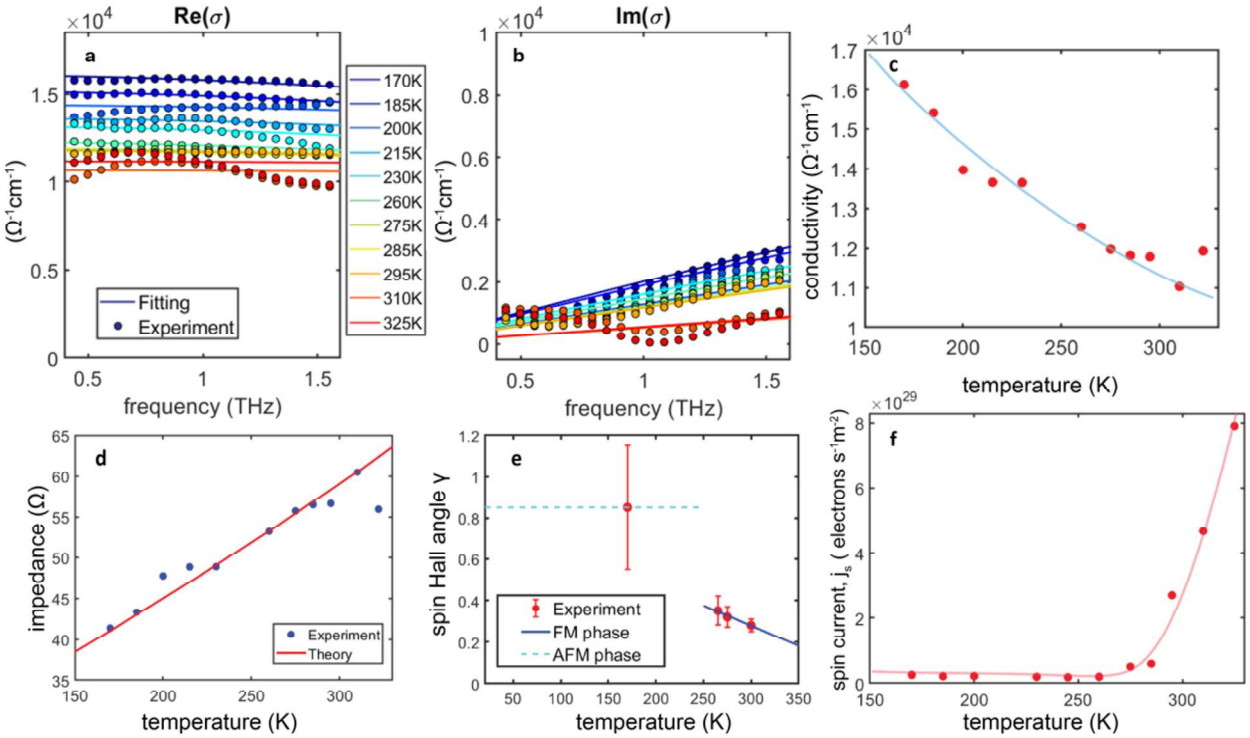

FIG. 3. (a) Real and (b) imaginary part of the optical conductivity of a 15 nm FeRh measured by time-domain THz transmission spectroscopy between 170 and 325 K. The conductivity (circular dots) is extracted by referencing a bare MgO substrate and fitted with a Drude model (solid lines). (c) DC conductivity of the 15 nm FeRh thin film extrapolated from (a). (d) Impedance of the 15 nm FeRh thin film extracted from the DC conductivity and thickness of the thin film. The data are fitted to a theoretical model proposed in Ref. 49. (e) Temperature dependent spin Hall angle extrapolated from spin-torque ferromagnetic resonance (FMR). Data adapted from Gibbons *et al.*[51] (f) Extracted light-induced spin current j_s as a function of temperature in the 15 nm FeRh film.

The spin Hall angle of FeRh is taken from measurements done by Gibbons *et al.*[51] Here, a DC-biased spin-torque ferromagnetic resonance (FMR) measurement on FeRh indicates that the FeRh samples have a surprisingly large spin Hall angle γ, and the spin direction in most of the samples is aligned with the magnetization direction. The value of γ is determined from the results measured between 170 and 300 K and extrapolated to a broader temperature range [Fig. 3(e)]. γ is measured to be 0.85 ±0.3 for the AFM state of FeRh at 170 K and assumed to be constant at lower temperatures. Across the phase transition point, γ decreases by ~3.5 times and decreases further with increasing temperature. The behavior of γ with temperature is roughly linear. Such a result is in agreement with a spin-torque FMR experiment done on the FM/AFM domains of FeRh,[52] in which the product of $\gamma\lambda_{rel}$ is measured to be 0.7 nm for the AFM state and 0.3 nm for the FM state. In pure metals, the spin relaxation length λ_{rel} is limited by impurity and phonon scattering.[53] Studies of the noble metals Pt and Au show that λ_{rel} is qualitatively higher at low temperatures[54] and remains in the same order between 170 and 300 K. Therefore, we assume that $\lambda_{rel} \sim 1$ nm for the above derivation.

By combining the above measured quantities, we can extract the light-induced spin current generated from a 15 nm FeRh thin film, as shown in Fig. 3(f). It is worth mentioning that we are overestimating the spin current in the FM phase of FeRh because our current model ignores the AHE and ANE contributions to the THz emission. In the AFM phase, the estimation is more accurate, and a small, temperature independent spin current is observed. This corresponds to the THz generated from the residual FM layer at the FeRh/MgO interface. The spin current undergoes a drastic enhancement across the phase transition point, becoming more pronounced and temperature dependent in the FM state due to a larger net magnetization of the bulk. Our study shows that the AFM state of FeRh, which exhibits no net magnetization, can still carry spin current, likely generated from the residual FM layer at the MgO–FeRh interface, and has a large SOC for the ISHE to occur to convert the spin current to a charge current. A possible future test for our hypothesis of the role of the residual FM later would consist of performing a systematic investigation of THz emission from FeRh grown on different substrates. Such future studies can help elucidate the origin of the spin current generation in the AFM phase of FeRh.

In summary, we performed temperature-dependent THz emission and time-domain THz spectroscopy in ferromagnetic and antiferromagnetic FeRh. We measured THz generation from bare FeRh thin film with no noble metal capping layer and extracted the light-induced spin current, j_s, for FeRh in both the AFM and the FM phases. Our findings provide insights into the ISHE mechanism inside magnetic materials, showing that for materials with strong spin–orbit coupling, the spin-to-charge current conversion can take place inside the FM layer and does not necessarily need a NM layer. This suggests that a careful evaluation of the ISHE process is needed for future studies of NM/FM THz emitters. Our findings and methods establish THz emission as a contact-less probe of spin current and spin current generation efficiency in magnetic materials. This method can be extended to study spin dynamics in more exotic condensed matter systems such as SC/FM heterostructures, hybrid magnon systems, and quantum spin liquids, which are otherwise hard to probe by conventional spectroscopic techniques.

ACKNOWLEDGMENTS

We thank Barry Bradlyn, Matthew Gilbert, and David Cahill for fruitful discussions.

This study was performed as part of the Illinois Materials Research Science and Engineering Center, supported by the National Science Foundation MRSEC program under NSF Award No. DMR-1720633.

Y. L. and F. M. acknowledge the support from the NSF Career Award No. DMR-2144256 (data analysis and manuscript preparation).

The preparation of the FeRh samples was supported as part of Quantum Materials for Energy Efficient Neuromorphic Computing (Q-MEEN-C), an Energy Frontier Research Center funded by the U.S. Department of Energy (DOE), Office of Science, Basic Energy Sciences (BES) under Award No. DE-SC 0019273.

AUTHOR DECLARATIONS

Conflict of Interest

The authors have no conflicts to disclose.

Author Contributions

Yinchuan Lv: Data curation (equal); Formal analysis (equal); Investigation (equal); Methodology (equal); Resources (equal); Software (equal); Validation (equal); Visualization (equal); Writing – original draft (equal); Writing – review & editing (equal). **Soho Shim**: Formal analysis (equal); Resources (equal); Validation (equal); Writing – review & editing (equal). **Jonathan Gibbons**: Formal analysis (equal); Resources (equal); Validation (equal); Writing – review & editing (equal). **Axel Hoffmann**: Formal analysis (equal); Funding acquisition (equal); Resources (equal); Validation (equal); Writing – review & editing (equal). **Nadya Mason**: Formal analysis (equal); Funding acquisition (equal); Resources (equal); Validation (equal); Writing – review & editing (equal). **Fahad Mahmood**: Conceptualization (equal); Data curation (equal); Formal analysis (equal); Funding acquisition (equal); Investigation (equal); Methodology (equal); Resources (equal); Software (equal); Supervision (equal); Validation (equal); Visualization (equal); Writing – original draft (equal); Writing – review & editing (equal).

DATA AVAILABILITY

The data that support the findings of this study are available from the corresponding author upon reasonable request.

REFERENCES

[1]T. Seifert, S. Jaiswal, U. Martens, J. Hannegan, L. Braun, P. Maldonado, F. Freimuth, A. Kronenberg, J. Henrizi, I. Radu *et al.*, "Efficient metallic spintronic emitters of ultrabroadband terahertz radiation," Nat. Photonics **10**, 483–488 (2016).

[2]T. Seifert, U. Martens, S. Günther, M. Schoen, F. Radu, X. Chen, I. Lucas, R. Ramos, M. H. Aguirre, P. A. Algarabel *et al.*, "Terahertz spin currents and inverse spin Hall effect in thin-film heterostructures containing complex magnetic compounds," *Spin* (World Scientific, 2017), Vol. 07, pp. 1740010

[3]T. Huisman, R. Mikhaylovskiy, J. Costa, F. Freimuth, E. Paz, J. Ventura, P. Freitas, S. Blügel, Y. Mokrousov, T. Rasing, and A. V. Kimel, "Femtosecond control of electric currents in metallic ferromagnetic heterostructures," Nat. Nanotechnol. **11**, 455–458 (2016).
[4]T. Seifert, S. Jaiswal, M. Sajadi, G. Jakob, S. Winnerl, M. Wolf, M. Kläui, and T. Kampfrath, "Ultrabroadband single-cycle terahertz pulses with peak fields of 300 kV cm^{-1} from a metallic spintronic emitter," Appl. Phys. Lett. **110**, 252402 (2017).
[5]T. S. Seifert, S. Jaiswal, J. Barker, S. T. Weber, I. Razdolski, J. Cramer, O. Gueckstock, S. F. Maehrlein, L. Nadvornik, S. Watanabe *et al.*, "Femtosecond formation dynamics of the spin Seebeck effect revealed by terahertz spectroscopy," Nat. Commun. **9**, 2899–2911 (2018).
[6]M. B. Jungfleisch, Q. Zhang, W. Zhang, J. E. Pearson, R. D. Schaller, H. Wen, and A. Hoffmann, "Control of terahertz emission by ultrafast spin-charge current conversion at Rashba interfaces," Phys. Rev. Lett. **120**, 207207 (2018).
[7]B. Miao, S. Huang, D. Qu, and C. Chien, "Inverse spin Hall effect in a ferromagnetic metal," Phys. Rev. Lett. **111**, 066602 (2013).
[8]H. Wang, C. Du, P. Chris Hammel, and F. Yang, "Spin current and inverse spin hall effect in ferromagnetic metals probed by $Y_3Fe_5O_{12}$-based spin pumping," Appl. Phys. Lett. **104**, 202405 (2014).
[9]N. Awari, A. Semisalova, J.-C. Deinert, K. Lenz, J. Lindner, E. Fullerton, V. Uhlíř, J. Li, B. Clemens, R. Carley *et al.*, "Monitoring laser-induced magnetization in FeRh by transient terahertz emission spectroscopy," Appl. Phys. Lett. **117**, 122407 (2020).
[10]W. Zhang, M. B. Jungfleisch, W. Jiang, J. E. Pearson, A. Hoffmann, F. Freimuth, and Y. Mokrousov, "Spin Hall effects in metallic antiferromagnets," Phys. Rev. Lett. **113**, 196602 (2014).
[11]T. Jungwirth, X. Marti, P. Wadley, and J. Wunderlich, "Antiferromagnetic spintronics," Nat. Nanotechnol. **11**, 231–241 (2016).
[12]Q. Shao, P. Li, L. Liu, H. Yang, S. Fukami, A. Razavi, H. Wu, K. Wang, F. Freimuth, Y. Mokrousov *et al.*, "Roadmap of spin-orbit torques," IEEE Trans. Magn. **57**, 1 (2021).
[13]G. Shirane, C. Chen, P. Flinn, and R. Nathans, "Hyperfine fields and magnetic moments in the Fe–Rh system," J. Appl. Phys. **34**, 1044–1045 (1963).
[14]C. Bordel, J. Juraszek, D. W. Cooke, C. Baldasseroni, S. Mankovsky, J. Minár, H. Ebert, S. Moyerman, E. Fullerton, and F. Hellman, "Fe spin reorientation across the metamagnetic transition in strained FeRh thin films," Phys. Rev. Lett. **109**, 117201 (2012).
[15]N. Baranov and E. Barabanova, "Electrical resistivity and magnetic phase transitions in modified FeRh compounds," J. Alloys Compd. **219**, 139–148 (1995).
[16]C. Baldasseroni, G. Pálsson, C. Bordel, S. Valencia, A. Unal, F. Kronast, S. Nemsak, C. Fadley, J. A. Borchers, B. B. Maranville, and F. Hellman, "Effect of capping material on interfacial ferromagnetism in FeRh thin films," J. Appl. Phys. **115**, 043919 (2014).
[17]L. Lewis, C. Marrows, and S. Langridge, "Coupled magnetic, structural, and electronic phase transitions in FeRh," J. Phys. D: Appl. Phys. **49**, 323002 (2016).
[18]A. Ceballos, Z. Chen, O. Schneider, C. Bordel, L.-W. Wang, and F. Hellman, "Effect of strain and thickness on the transition temperature of epitaxial FeRh thin-films," Appl. Phys. Lett. **111**, 172401 (2017).
[19]G. Ju, J. Hohlfeld, B. Bergman, R. J. van de Veerdonk, O. N. Mryasov, J.-Y. Kim, X. Wu, D. Weller, and B. Koopmans, "Ultrafast generation of ferromagnetic order via a laser-induced phase transformation in FeRh thin films," Phys. Rev. Lett. **93**, 197403 (2004).
[20]J.-U. Thiele, M. Buess, and C. H. Back, "Spin dynamics of the antiferromagnetic-to-ferromagnetic phase transition in FeRh on a sub-picosecond time scale," Appl. Phys. Lett. **85**, 2857–2859 (2004).
[21]B. Bergman, G. Ju, J. Hohlfeld, R. J. van de Veerdonk, J.-Y. Kim, X. Wu, D. Weller, and B. Koopmans, "Identifying growth mechanisms for laser-induced magnetization in FeRh," Phys. Rev. B **73**, 060407 (2006).
[22]A. Gray, D. Cooke, P. Krüger, C. Bordel, A. Kaiser, S. Moyerman, E. Fullerton, S. Ueda, Y. Yamashita, A. Gloskovskii *et al.*, "Electronic structure changes across the metamagnetic transition in FeRh via hard X-ray photoemission," Phys. Rev. Lett. **108**, 257208 (2012).
[23]C. Stamm, J.-U. Thiele, T. Kachel, I. Radu, P. Ramm, M. Kosuth, J. Minár, H. Ebert, H. Dürr, W. Eberhardt, and C. H. Back, "Antiferromagnetic-ferromagnetic phase transition in FeRh probed by X-ray magnetic circular dichroism," Phys. Rev. B **77**, 184401 (2008).
[24]J. Cao, N. T. Nam, S. Inoue, H. Y. Y. Ko, N. N. Phuoc, and T. Suzuki, "Magnetization behaviors for FeRh single crystal thin films," J. Appl. Phys. **103**, 07F501 (2008).
[25]F. Pressacco, D. Sangalli, V. Uhlíř, D. Kutnyakhov, J. A. Arregi, S. Y. Agustsson, G. Brenner, H. Redlin, M. Heber, D. Vasilyev *et al.*, "Subpicosecond metamagnetic phase transition in FeRh driven by non-equilibrium electron dynamics," Nat. Commun. **12**, 5088 (2021).
[26]I. Dolgikh, T. Blank, G. Li, K. Prabhakara, S. Patel, A. Buzdakov, R. Medapalli, E. Fullerton, O. Koplak, J. Mentink *et al.*, "Ultrafast emergence of ferromagnetism in antiferromagnetic FeRh in high magnetic fields," arXiv:2202.03931 (2022).
[27]S. Maat, J.-U. Thiele, and E. E. Fullerton, "Temperature and field hysteresis of the antiferromagnetic-to-ferromagnetic phase transition in epitaxial FeRh films," Phys. Rev. B **72**, 214432 (2005).
[28]R. Medapalli, G. Li, S. K. Patel, R. Mikhaylovskiy, T. Rasing, A. Kimel, and E. Fullerton, "Femtosecond photocurrents at the FeRh/Pt interface," Appl. Phys. Lett. **117**, 142406 (2020).
[29]X. Xie, J. Xu, and X.-C. Zhang, "Terahertz wave generation and detection from a CdTe crystal characterized by different excitation wavelengths," Opt. Lett. **31**, 978–980 (2006).
[30]X. Ropagnol, M. Matoba, J. E. Nkeck, F. Blanchard, E. Isgandarov, J. Yumoto, and T. Ozaki, "Efficient terahertz generation and detection in cadmium telluride using ultrafast ytterbium laser," Appl. Phys. Lett. **117**, 181101 (2020).
[31]S. Kim, Y. Lv, X.-Q. Sun, C. Zhao, N. Bielinski, A. Murzabekova, K. Qu, R. A. Duncan, Q. L. D. Nguyen, M. Trigo, D. P. Shoemaker, B. Bradlyn, and F. Mahmood, "Observation of a massive phason in a charge-density-wave insulator," Nat. Mater. **22**, 429–433 (2023).
[32]G. Li, R. Medapalli, J. Mentink, R. Mikhaylovskiy, T. Blank, S. Patel, A. Zvezdin, T. Rasing, E. Fullerton, and A. Kimel, "Ultrafast kinetics of the antiferromagnetic-ferromagnetic phase transition in ferh," Nat. Commun. **13**, 2998 (2022).
[33]C. Baldasseroni, C. Bordel, A. Gray, A. Kaiser, F. Kronast, J. Herrero-Albillos, C. Schneider, C. Fadley, and F. Hellman, "Temperature-driven nucleation of ferromagnetic domains in FeRh thin films," Appl. Phys. Lett. **100**, 262401 (2012).
[34]S. Mariager, L. L. Guyader, M. Buzzi, G. Ingold, and C. Quitmann, "Imaging the antiferromagnetic to ferromagnetic first order phase transition of FeRh," arXiv:1301.4164 (2013).
[35]Z. Feng, W. Tan, Z. Jin, Y.-J. Chen, Z. Zhong, L. Zhang, S. Sun, J. Tang, Y. Jiang, P.-H. Wu *et al.*, "Anomalous Nernst effect induced terahertz emission in a single ferromagnetic film," Nano Lett. **23**, 8171–8179 (2023).
[36]A. Popescu, P. Rodriguez-Lopez, P. M. Haney, and L. M. Woods, "Thermally driven anomalous Hall effect transitions in FeRh," Phys. Rev. B **97**, 140407 (2018).
[37]T. Higuchi, N. Kanda, H. Tamaru, and M. Kuwata-Gonokami, "Selection rules for light-induced magnetization of a crystal with threefold symmetry: The case of antiferromagnetic NiO," Phys. Rev. Lett. **106**, 047401 (2011).
[38]H. Qiu, L. Zhou, C. Zhang, J. Wu, Y. Tian, S. Cheng, S. Mi, H. Zhao, Q. Zhang, D. Wu *et al.*, "Ultrafast spin current generated from an antiferromagnet," Nat. Phys. **17**, 388–394 (2021).
[39]H. Zhang, Z. Feng, G. Li, L. Zhang, X. Chen, H. Bai, S. Sun, J. Tang, J. Zhang, F. Han *et al.*, "Tuning terahertz emission generated by anomalous Nernst effect in ferromagnetic metal," Appl. Phys. Rev. **10**, 021417 (2023).
[40]Q. Zhang, Z. Luo, H. Li, Y. Yang, X. Zhang, and Y. Wu, "Terahertz emission from anomalous hall effect in a single-layer ferromagnet," Phys. Rev. Appl. **12**, 054027 (2019).
[41]F. Quirin, M. Vattilana, U. Shymanovich, A.-E. El-Kamhawy, A. Tarasevitch, J. Hohlfeld, D. von der Linde, and K. Sokolowski-Tinten, "Structural dynamics in FeRh during a laser-induced metamagnetic phase transition," Phys. Rev. B **85**, 020103 (2012).
[42]R. Fan, C. J. Kinane, T. Charlton, R. Dorner, M. Ali, M. De Vries, R. M. Brydson, C. H. Marrows, B. J. Hickey, D. A. Arena *et al.*, "Ferromagnetism at the interfaces of antiferromagnetic FeRh epilayers," Phys. Rev. B **82**, 184418 (2010).

[43]F. Pressacco, V. Uhlíř, M. Gatti, A. Bendounan, E. E. Fullerton, and F. Sirotti, "Stable room-temperature ferromagnetic phase at the FeRh (100) surface," Sci. Rep. **6**, 1–9 (2016).
[44]C. Gatel, B. Warot-Fonrose, N. Biziere, L. Rodríguez, D. Reyes, R. Cours, M. Castiella, and M.-J. Casanove, "Inhomogeneous spatial distribution of the magnetic transition in an iron-rhodium thin film," Nat. Commun. **8**, 15703–15708 (2017).
[45]M. Menarini, R. Medapalli, E. E. Fullerton, and V. Lomakin, "Micromagnetic simulation of THz signals in antiferromagnetic FeRh by sub-picosecond thermal pulses," AIP Adv. **9**, 035040 (2019).
[46]G.-M. Choi, B.-C. Min, K.-J. Lee, and D. G. Cahill, "Spin current generated by thermally driven ultrafast demagnetization," Nat. Commun. **5**, 4334–4338 (2014).
[47]G.-M. Choi, C.-H. Moon, B.-C. Min, K.-J. Lee, and D. G. Cahill, "Thermal spin-transfer torque driven by the spin-dependent Seebeck effect in metallic spin-valves," Nat. Phys. **11**, 576–581 (2015).
[48]H. Saglam, C. Liu, Y. Li, J. Sklenar, J. Gibbons, D. Hong, V. Karakas, J. E. Pearson, O. Ozatay, W. Zhang *et al.*, "Anomalous Hall and Nernst effects in FeRh," arXiv:2012.14383 (2020).
[49]S. Mankovsky, S. Polesya, K. Chadova, H. Ebert, J. Staunton, T. Gruenbaum, M. Schoen, C. Back, X. Chen, and C. Song, "Temperature-dependent transport properties of FeRh," Phys. Rev. B **95**, 155139 (2017).
[50]P. Tu, A. Heeger, J. Kouvel, and J. Comly, "Mechanism for the first-order magnetic transition in the FeRh system," J. Appl. Phys. **40**, 1368–1369 (1969).
[51]J. Gibbons, T. Dohi, V. P. Amin, F. Xue, H. Ren, J.-W. Xu, H. Arava, S. Shim, H. Saglam, Y. Liu *et al.*, "Large exotic spin torques in antiferromagnetic iron rhodium," arXiv:2109.11108 (2021).
[52]Y. Wang, M. M. Decker, T. N. Meier, X. Chen, C. Song, T. Grünbaum, W. Zhao, J. Zhang, L. Chen, and C. H. Back, "Spin pumping during the antiferromagnetic–ferromagnetic phase transition of iron–rhodium," Nat. Commun. **11**, 275–278 (2020).
[53]J. Bass and W. P. Pratt, "Spin-diffusion lengths in metals and alloys, and spin-flipping at metal/metal interfaces: An experimentalist's critical review," J. Phys.: Condens. Matter **19**, 183201 (2007).
[54]M. Isasa, E. Villamor, L. E. Hueso, M. Gradhand, and F. Casanova, "Temperature dependence of spin diffusion length and spin Hall angle in Au and Pt," Phys. Rev. B **91**, 024402 (2015).